

Designing Multi-Rotor Tidal Turbine Fences

C. R. Vogel, R. H. J. Willden

Department of Engineering Science, University of Oxford

Parks Road, Oxford OX1 3PJ

E-mail: christopher.vogel@eng.ox.ac.uk

Abstract—An embedded Reynolds-Averaged Navier-Stokes blade element actuator disk model is used to investigate the hydrodynamic design of tidal turbines and their performance in a closely spaced cross-stream fence. Turbines designed for confined flows are found to require a larger blade solidity ratio than current turbine design practices imply in order to maximise power. Generally, maximum power can be increased by operating turbines in more confined flows than they were designed for, although this also requires the turbines to operate at a higher rotational speed, which may increase the likelihood of cavitation inception. In-array turbine performance differs from that predicted from single turbine analyses, with cross-fence variation in power and thrust developing between the inboard and outboard turbines. As turbine thrust increases the cross-fence variation increases, as the interference effects between adjacent turbines strengthen as turbine thrust increases, but it is observed that cross-stream variation can be mitigated through strategies such as pitch-to-feather power control. It was found that overall fence performance was maximised by using turbines designed for moderately constrained (blocked) flows, with greater blockage than that based solely on fence geometry, but lower blockage than that based solely on the turbine and local flow passage geometry to balance the multi-scale flow phenomena around tidal fences.

Index Terms—Tidal stream turbines, tidal turbine arrays, power capping, tidal turbine design, blade element theory

I. INTRODUCTION

The importance of the blockage ratio, the ratio of turbine swept area to the cross-sectional area of the flow passage surrounding the turbine, B_L , was established in the context of tidal stream turbine performance by Garrett and Cummins [1]. For turbines idealised as actuator disks, it was demonstrated that the theoretical peak power coefficient increases by a factor $(1 - B_L)^{-2}$ above the Betz limit, $C_P = 16/27$. The flow passage boundaries around a turbine occur not only as a result of the flow confinement due to the seabed, sea-surface, and channel walls, but may also arise due to the presence of adjacent turbines that constrain the flow expansion around the turbines. The theoretical power coefficient limit increases as a consequence of a streamwise static pressure (head) difference developing in the flow passage due to momentum extraction by the actuator disk and mass conservation requirements. The static pressure difference that can be supported in the flow passage increases with the blockage ratio, and thus the increase in maximum power coefficient is achieved at higher thrust levels and lower through-disk flow speeds.

Theoretical and numerical studies on tidal turbine efficiency have confirmed and extended the work of Garrett and Cummins to configurations of multiple turbines in side-by-side and staggered arrangements, as well as exploring the

role of multi-scale hydrodynamics when the turbine fence does not completely span the channel cross-section [2]–[5]. In the context of multi-turbine arrays occupying a fraction of a wider tidal flow passage, it is also useful to define the global blockage ratio, B_G , as the ratio of the frontal area of all turbines in an array to the cross-sectional area of the tidal flow passage in order to describe the multi-scale flow phenomena that arise.

It has been demonstrated that exploiting the uplift in turbine performance theoretically available in blocked conditions requires turbines to be designed specifically to support the higher levels of thrust required to access the improved levels of available power [6]. Schluntz and Willden designed turbines to optimise turbine hydrodynamic performance for a specified local blockage ratio with a uniform inflow velocity. It was found that the higher levels of thrust required to realise the theoretically available increase in turbine power may be achieved through two broad routes; operating turbines at higher tip speed ratios, or redesigning the rotor to increase the solidity ratio. Amongst the constraints on the rotor design process is that the rotational speed of the turbine must be limited to avoid cavitation inception along the blade, which restricts the range of operational tip speed ratios.

Recent work has highlighted further challenges in designing short fences of turbines as a result of cross-stream variations in the level of thrust and power across the fence. Actuator disk experiments by [7] showed that the turbine thrust and power reduce towards the ends of the fence, which can be significantly detrimental to the overall power of a short fence of turbines. This is also reflected in the non-uniform flow speeds observed across the fence. Nishino and Willden [5] discussed similar effects in analytic and computational models of short tidal fences. However, there lacks at present a simple, tractable model to predict the decrease in thrust and power at the ends of a finite length fence and the ensuing design implications for tidal stream turbine design.

This work addresses the question of turbine design within short cross-stream fences of tidal turbines. The potential performance uplift from closely spacing turbines has been demonstrated in the work discussed above, but the design process to best exploit the potential performance uplift remains unclear. This work investigates the role of flow phenomena that scale on the turbine diameter and array width, described by the local and global blockage ratios respectively, on overall multi-rotor fence power and thrust characteristics. Turbines are hydrodynamically designed for a range of local blockage

ratios. The turbines are then tested in a multi-rotor fence configuration, where the inter-turbine spacing is held constant at a representative tip-to-tip spacing of one turbine diameter, as might be found in a closely-packed turbine fence. It is shown that the interactions between adjacent turbines, and hence design considerations, are a function of the thrust of the adjacent turbines, and consequently it is not sufficient to exclusively consider just the local blockage ratio or the global blockage ratio in the turbine design process.

The analysis in this paper is broken into four stages. Firstly, single turbines were hydrodynamically designed by varying blade twist and solidity ratios for operation under five different blockage conditions with a fixed tip speed ratio. Performance of the turbines was then analysed for a range of different tip speed ratios and off-design blockage conditions. These turbines were then arranged in a cross-stream tidal fence arrayed normal to the flow direction in order to study the relative importance of global and local blockage ratios. Finally, the effect of pitch-to-feather power control on array performance was investigated.

II. NUMERICAL MODEL

The numerical simulations in this study were performed using the commercial CFD solver ANSYS Fluent, v.15.0, solving the 3D incompressible Reynolds-Averaged Navier-Stokes (RANS) equations with a finite volume method. The simulations were performed as steady computations, with turbulence closure provided by the $k - \omega$ SST model, which combines the advantages of the $k - \omega$ model near no-slip boundaries, such as the nacelle, with the $k - \epsilon$ model in the remainder of the domain. The $k - \omega$ SST model has been widely used in both marine and wind turbine studies [8].

The tidal turbines were modelled as actuator disks, using the ‘fan’ internal boundary condition in Fluent. User defined functions, following [9], were used to implement a RANS-embedded Blade Element Actuator Disk (RANS-BE AD) model, which sampled the numerically simulated flow field at the location of the actuator disk. The flow field data, in conjunction with the rotor geometry and aerofoil data, were used to calculate the azimuthally-averaged axial and tangential forces acting on each spanwise section of the rotor blades using blade element theory. The spanwise azimuthally-varying forces were in turn imposed on the flow as a static pressure discontinuity and a change in swirl velocity across the actuator disk. The modelling differences between the three-bladed rotors and the actuator disks being simulated (which can be approximated as rotors with infinitely many blades) were accounted for using the Glauert implementation of the Prandtl tip loss model, see [10]. The tip loss model is used to reconcile the difference in flow speed incident on the rotor blades with the azimuthally-averaged flow speed through the actuator disk, and is applied to the blade element calculations using the axial flow speed computed in the numerical simulations.

All the rotors simulated in this work had a diameter $d = 20\text{m}$, three blades, and a nacelle of diameter $0.15d$. The nacelle has a hemispherical nose and tail, and is $0.5d$ in length.

TABLE I
ROTOR DESIGN CONFIGURATIONS

Name	B_L	s/d
Case 1	0.0001	$\rightarrow \infty$
Case 2	0.0357	10
Case 3	0.0507	6.75
Case 4	0.0650	5
Case 5	0.1960	1

For simplicity, the rest of the rotor support structure was not simulated. Following [6], the rotor aerofoil section used herein is the Risø A1-24, a 24% thickness aerofoil section with good lift-to-drag characteristics [11], with the maximum lift-to-drag ratio occurring at an angle of attack $\alpha = 5^\circ$. A uniform inflow velocity of $u_\infty = 2\text{ms}^{-1}$ was applied to the inlet of all the simulations, with seawater ($\rho = 1025\text{kgm}^{-3}$) as the working fluid.

A. Single Rotor Computations

A series of single turbine computations were performed in cylindrical domains to design and then evaluate the off-design performance of the three-bladed turbines, designed for a range of local blockage ratios. The mesh was block-structured, consisting of hexahedral elements. The resolution at the rotor plane varied across the disk face in order to provide higher resolution at the disk edge, with the minimum element length $\epsilon_{min} = 1/135d$, and the maximum element length on the disk plane $\epsilon_{max} = 1/30d$. A streamwise growth rate of 1.1 was used for the elements in the wake region. The overall number of elements in the mesh was approximately 1×10^6 , varying slightly with domain radius according to blockage ratio. The simulations were run for 5000 iterations to ensure that normalised residuals were below 10^{-5} .

The rotor design procedure adjusts, for a given tip speed ratio, the blade twist angle and solidity ratio along the blade to target a prescribed angle of attack (in order to achieve the maximum 2D aerofoil lift-to-drag ratio, 5° for the Risø A1-24 aerofoil) and a specified local thrust coefficient. The local thrust coefficient $C_x = \Delta F_x / \frac{1}{2} \rho u_x^2$, where ΔF_x is the applied axial force per unit area, ρ is the fluid density, and u_x is the axial flow speed through the rotor plane. For simplicity, the local thrust coefficient is specified to be constant along the blade span. A maximum solidity ratio (ratio of net local blade chord to circumference at a given radial station) of $\sigma = 1.50$ was set to ensure numerical stability of the design algorithm and that the blades did not overlap at the root when blade twist was taken into account. After the numerical design process was completed, following [12], sections of the blade designs inboard of a relative position of $r/R = 0.26$ were tapered to a cylindrical section at the root, resulting in a reduction in blade twist angle and solidity ratio.

Five single rotor blockage ratios were considered, as summarised in Table I. The tip-to-tip spacing ratio s/d is given for comparison to the equivalent design conditions in the multi-rotor configuration (discussed below) where the water depth

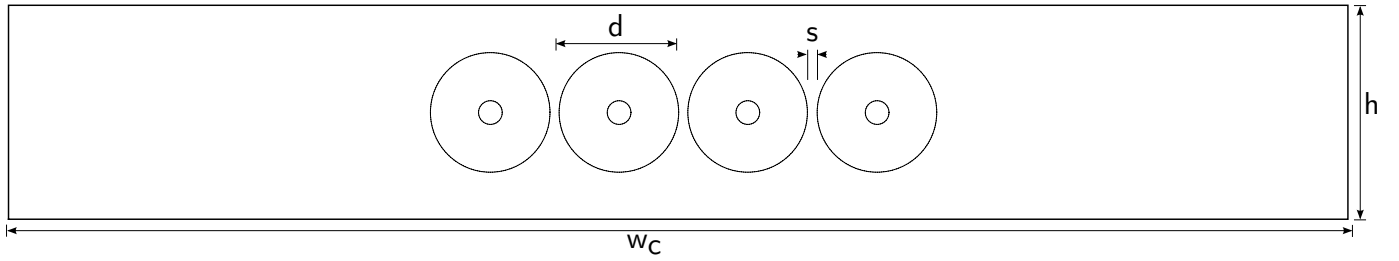


Fig. 1. Diagram of the computational domain for the four rotor fence at the rotor plane. d is the turbine diameter, s is the inter-turbine tip-to-tip spacing, h is the channel depth, and w_c is the channel width.

is fixed at $2d$. Two of the cases, Cases 1 and 5, $B_L = \frac{1}{4}\pi d^2/h(s+d) = 0.0001$ and $B_L = 0.1960$ respectively, were matched to the designs of [6]. Case 3 was selected to match the global blockage ratio, $B_G = n\frac{1}{4}\pi d^2/w_c h = 0.0507$, where n is the number of turbines, of the multi-rotor computations, and Cases 2 and 4 were selected to represent intermediate spacing ratios of $s/d = 5$ and 10 that correspond to blockage ratios slightly larger and slightly smaller than the global blockage ratio.

B. Multi-rotor Computations

The multi-rotor simulations of four identical turbines were performed using a rectangular computational domain. The actuator disks were positioned normal to the flow direction in a cross-stream array (in the yz -plane) centred on $x = y = z = 0$ in a configuration as illustrated in Figure 1 with an inter-turbine tip-to-tip spacing ratio of $s/d = 1$. The channel depth was $h = 2d$, the channel width was $w_c = 31d$, and the domain extended $17d$ upstream and $55d$ downstream of the rotor fence. Slip wall boundary conditions were applied to the top and bottom boundaries of the domain, meaning that the free surface of the fluid was modelled as a rigid lid, and symmetric boundary conditions were applied to the lateral walls. Following a mesh-sensitivity study, the multi-rotor domain contained approximately 7×10^6 elements.

It was assumed in the multi-rotor fence simulations that the turbines in the fence were identical and contra-rotating. Five sets of multi-rotor simulations were performed; one for each of the five rotor designs determined in the single turbine cases. Despite the changing design blockage for the turbines, the local and global blockage of the multi-rotor fence remained constant, $B_L = 0.1960$ and $B_G = 0.0507$ respectively.

III. SINGLE ROTOR DESIGN AND PERFORMANCE

The design algorithm was executed over a range of local thrust coefficients $1.80 \leq C_x \leq 3.80$ for a fixed tip speed ratio $\lambda = \Omega R/u_\infty = 5$, where Ω is the rotational speed of the rotor and $R = d/2$ is the tip radius. The peak power coefficient $C_P = P/\frac{1}{2}\rho u_\infty^3 A_d$, where P is turbine power, and A_d is the rotor swept area, was achieved at higher local thrust coefficients as the blockage ratio was increased, rising from a local thrust coefficient of $C_x = 2.00$ in Case 1 ($B_L = 0.0001$), to $C_x = 2.70$ in Case 3 ($B_L = 0.0507$), and $C_x = 3.20$ in Case 5 ($B_L = 0.1960$).

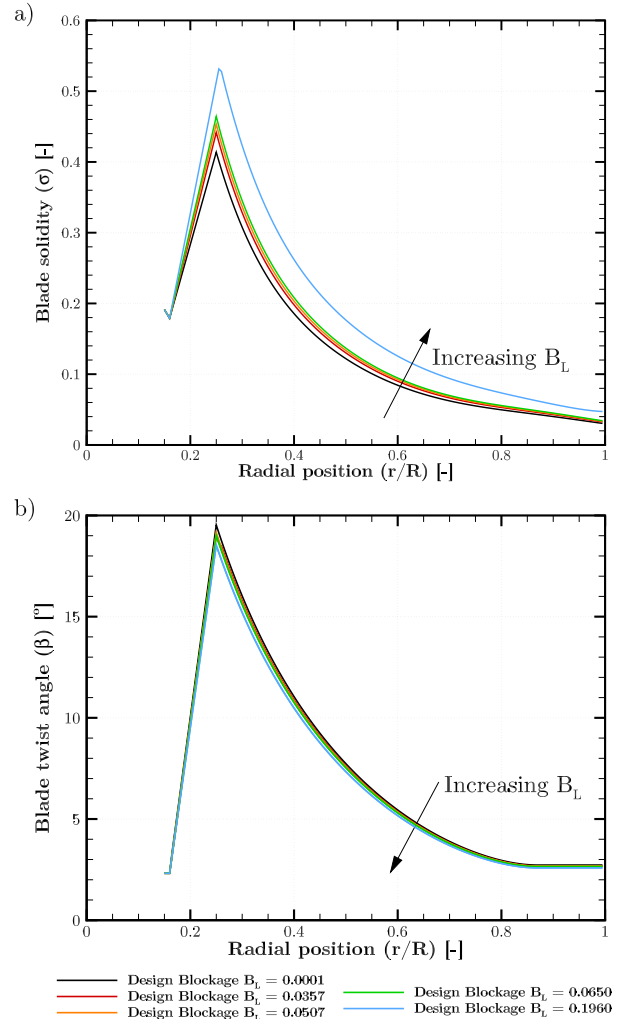


Fig. 2. Blade solidity, σ , (a) and blade twist angle, β , (b) for the five rotor designs for local blockage ratios $B_L = 0.0001$ (black), $B_L = 0.0357$ (red), $B_L = 0.0507$ (orange), $B_L = 0.0650$ (green), and $B_L = 0.1960$ (blue). Solidity increases with increasing B_L , whereas the blade twist angle reduces.

The maximum turbine power coefficient increases with the target local thrust coefficient as the blockage ratio is increased because increasing the blockage ratio means that the flow passage bypassing the turbine is increasingly constrained, resulting in a greater acceleration of the bypass flow. This

results in a reduction in the static pressure in the bypass flow, and hence, when hydrostatic pressure equalisation occurs between the bypass flow and the core flow in the wake of the device, there is a lower static pressure downstream of the turbine as well. The greater static pressure difference that consequently develops across the rotor plane means that, for a given mass flow rate through the turbine, turbines in higher blockage ratio configurations are able to apply a greater thrust to the flow, and hence achieve a higher power coefficient than lower blockage turbines. Therefore, as the blockage ratio increases, the peak power coefficient is achieved at a higher level of local thrust coefficient (and hence turbine thrust) as the flow is able to sustain a higher level of resistance before becoming choked by the turbine.

Turbine thrust is a function of the rotational speed of the rotor and the design of the rotor blades. Thrust increases as the rotational speed is increased as well as if the rotor blades are designed to present a greater resistance to the incoming flow. Fixing the rotational speed of the turbine by specifying the design tip speed ratio $\lambda = 5$ means that rotor geometry is the only available degree of freedom, with the final rotor designs for the five blockage ratios shown in Figure 2. The design rotor solidity, $\sigma = N_B c(r)/2\pi r$, where $N_B = 3$ is the number of turbine blades and $c(r)$ is the blade chord at radius r , increases as the blockage ratio increases in order to achieve the higher local thrust coefficient and hence higher rotor thrust that is required to increase the power coefficient. The solidity ratio increases linearly away from the hub for radial stations $r/R < 0.26$ in order to transition the rotor design between cylindrical base at the hub and the solution proposed by the design algorithm, following [12]. There is a much smaller variation in blade twist angle β between the different blockage ratio designs, with a reduction in blade twist angle of up to 1° between the designs in Case 1 ($B_L = 0.0001$) and Case 5 ($B_L = 0.1960$).

Figure 3 shows the variation in power coefficient, C_P , and thrust coefficient, C_T , with tip speed ratio for the five rotors, operating in domains with the respective blockage ratios that the rotors were designed for. For a given tip speed ratio, the thrust coefficient increases with the local blockage ratio as the increasing volume flow constraint results in a greater acceleration of the bypass flow and sustains higher flow speeds through the rotor plane. The higher flow speed through the rotor plane means that the relative velocity on the blades is higher, producing larger axial and tangential forces, and hence the thrust and power coefficients increase.

The maximum power coefficient increases from $C_P = 0.493$ for Case 1 ($B_L = 0.0001$) to $C_P = 0.752$ for Case 5, where $B_L = 0.1960$, an increase of 52.5%, and the corresponding thrust coefficient at the maximum power coefficients increases from $C_T = 0.975$ to $C_T = 1.381$ respectively, an increase of 45.8%. The tip speed ratio at which the maxima occur increases from $\lambda = 5.83$ in Case 1 to $\lambda = 6.08$ for Case 5. Although the rotors were hydrodynamically optimised for a fixed tip speed ratio $\lambda = 5.00$, the power coefficient is maximised for the rotor designs at tip speed ratios greater

than $\lambda = 5.00$ because of the increased relative flow speed incident on the turbine blades. However, a turbine designed for operation at the higher tip speed ratios would achieve an even higher power coefficient.

A. Off-Design Rotor Performance

Figure 4 compares the performance of three different design cases; Cases 1, 3, and 5, in domains of blockage ratio $B_L = 0.0001$, $B_L = 0.0507$, and $B_L = 0.1960$. Turbine power is dependent on the resistance that the turbine presents to the flow, and it was shown previously that the turbine thrust required to maximise the power coefficient increased as the blockage ratio the turbine operates in increased. Consequently, to achieve a given level of power, turbines designed for operation in lower blockage (Cases 1 and 3, for example) must generally operate at a higher rotational speed than higher blockage ratio turbine designs (such as Case 5), regardless of the blockage ratio due to the difference in the solidity ratio of the designs. The high level of thrust of the high blockage ratio turbine design reduces the approach flow speed more significantly than lower blockage ratio designs. Hence the high blockage ratio turbine, for a given, small, tip speed ratio, operates at an angle of attack closer to that required to maximise the lift-to-drag ratio, as compared to the lower blockage ratio designs. Consequently the high blockage ratio design achieves the highest power coefficient at low tip speed ratios in all domains of the three different rotor designs.

Increasing the tip speed ratio results in a reduction in the angle of attack on the blades, which affects the ratio of the tangential forces (which generate torque) to the axial forces of the different designs. For a given rotational speed, the angle of attack along the blade span generally reduces as the design blockage ratio of the turbine increases, giving rise to the differing performance of the rotors. Therefore, as the tip speed ratio increases the rotor achieving an angle of attack along most of the blade span closest to the optimal value to maximise the lift-to-drag ratio transitions from the highest blockage turbine design, Case 5, to the moderate blockage turbine design, Case 3, to the lowest blockage turbine design, Case 1. The rotor design to achieve the maximum power coefficient in a given blockage ratio domain also changes in that order.

Although increasing the rotational speed of lower blockage designs enables them to achieve higher power coefficients, approaching those of higher blockage designs, the drag forces acting on the rotor blades are relatively larger than those acting on the blades of the rotor designed for operation in high blockage ratios when the power coefficient is maximised. As shown in Table II, the maximum power coefficient of the Case 5 (high blockage ratio design) turbine in the $B_L = 0.1960$ domain is higher, $C_P = 0.752$ and achieved at a lower tip speed ratio, $\lambda = 6.08$, than the maximum power coefficient in the same domain of $C_P = 0.729$, when $\lambda = 6.56$ of the Case 3 turbine, and $C_P = 0.717$ of the Case 1 (zero blockage ratio design) turbine, achieved at a higher tip speed ratio $\lambda = 6.77$. Similarly, the ratio of lift-to-drag forces on

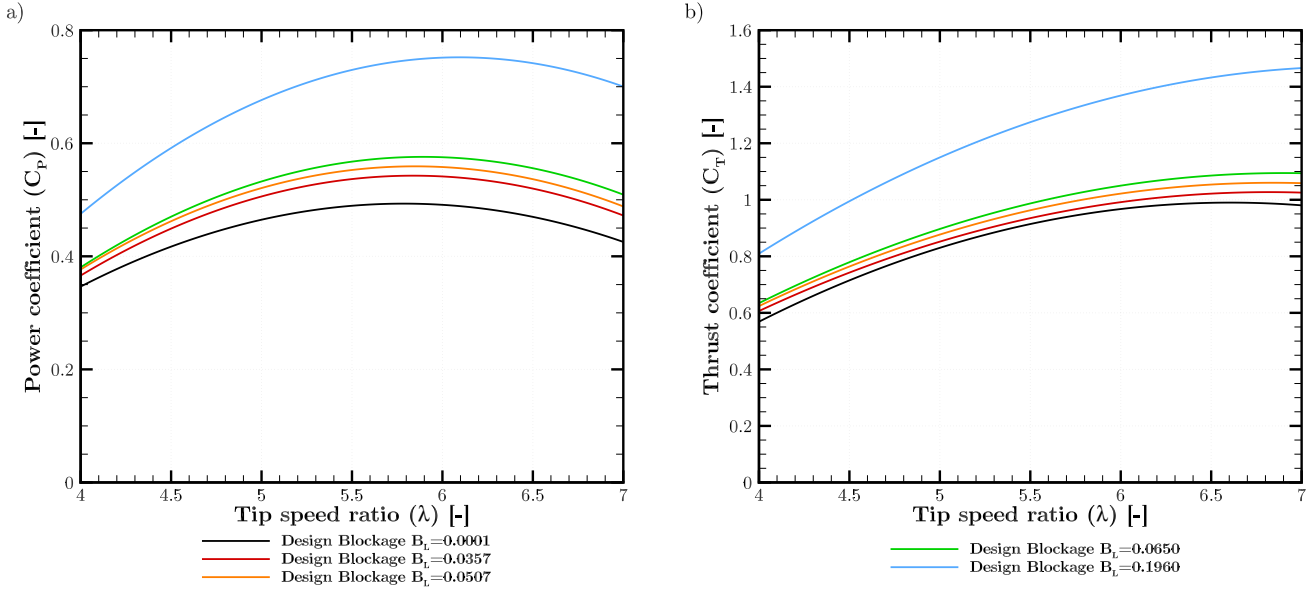


Fig. 3. Variation in (a) rotor power coefficient, C_P , and (b) thrust coefficient, C_T , with tip speed ratio λ for the five rotors designed for local blockage ratios $B_L = 0.0001$ (black), $B_L = 0.0357$ (red), $B_L = 0.0507$ (orange), $B_L = 0.0650$ (green), and $B_L = 0.1960$ (blue), operating in their respective design blockage ratios.

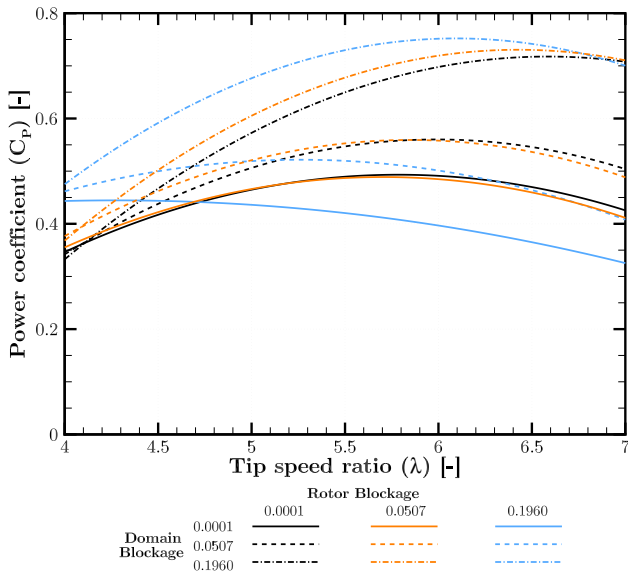


Fig. 4. Variation in rotor power coefficient C_P with tip speed ratio λ for three rotor designs for local blockage ratios: Case 1 $B_L = 0.0001$ (black), Case 3 $B_L = 0.0507$ (orange), and Case 5 $B_L = 0.1960$ (blue) in domains of blockage ratio $B_L = 0.0001$ (solid), $B_L = 0.0507$ (dashed), and $B_L = 0.1960$ (dot-dashed).

the different rotor designs means that in the $B_L = 0.0001$ domain the maximum power coefficient achieved by the Case 5 turbine is $C_P = 0.351$ at a tip speed ratio $\lambda = 4.20$ and $C_P = 0.489$ at a tip speed ratio of $\lambda = 5.70$ for the Case 3 turbine, as compared to a peak of $C_P = 0.493$ at $\lambda = 5.83$ for the Case 1 turbine.

TABLE II
MAXIMUM POWER COEFFICIENT AND CORRESPONDING TIP SPEED RATIO FOR ROTOR DESIGNS 1, 3, AND 5, IN DOMAINS WITH BLOCKAGE RATIOS $B_L = 0.0001$, $B_L = 0.0507$, AND $B_L = 0.1960$.

Domain Blockage	Rotor Design Case		
	1	3	5
0.0001	$C_P = 0.493$, $\lambda = 5.83$	$C_P = 0.489$, $\lambda = 5.74$	$C_P = 0.351$, $\lambda = 4.20$
0.0507	$C_P = 0.559$, $\lambda = 5.94$	$C_P = 0.559$, $\lambda = 5.81$	$C_P = 0.522$, $\lambda = 5.25$
0.1960	$C_P = 0.717$, $\lambda = 6.77$	$C_P = 0.729$, $\lambda = 6.56$	$C_P = 0.752$, $\lambda = 6.08$

There is less than a 5% variation in maximum power coefficient between the three turbine design cases, 1, 3, and 5, with an over 11% variation in corresponding tip speed ratio in the $B_L = 0.1960$ domain. The differences in blade design and tip speed ratio for the three cases required to achieve the peak power coefficient mean that there is a significantly different angle of attack distribution in the spanwise direction along the blades, with higher angle of attack being associated with lower blockage designs. The angle of attack at the $r/R = 0.80$ radial station is $\alpha = 4.43^\circ$ for the Case 1 turbine, reducing to $\alpha = 4.28^\circ$ for the Case 3 turbine, and $\alpha = 4.11^\circ$ for the Case 5 turbine. Hence, following the analysis proposed by [13], cavitation inception is more likely to occur on the blades of lower blockage designs when the turbines are operated to maximise the power coefficient, as the tip speed ratio required to achieve peak performance is higher. The computational analysis conducted herein demonstrates that turbines designed

TABLE III
 ROTOR POWER COEFFICIENT AND CORRESPONDING TIP SPEED RATIO AND THRUST COEFFICIENT FOR THE FIVE ROTOR DESIGNS IN THE MULTI-ROTOR FENCE CONFIGURATION WHEN FENCE POWER IS MAXIMISED.

Domain Blockage	Inboard			Outboard		
	C_P	C_T	λ	C_P	C_T	λ
0.0001	0.581	0.995	5.94	0.578	0.992	5.94
0.0357	0.582	1.004	5.79	0.578	1.001	5.79
0.0507	0.583	1.015	5.75	0.579	1.011	5.75
0.0650	0.585	1.027	5.72	0.580	1.023	5.72
0.1960	0.536	1.083	4.73	0.528	1.075	4.73

for low blockage configurations can achieve a significant proportion of the performance increment available to turbines designed to exploit constrained flow conditions. However, operational constraints (cavitation as well as drive train) may restrict the maximum operating speed of the turbine. The performance improvement available to low blockage turbine designs when operating in higher blockage configurations, achieved by operating the turbines at higher tip speed ratios, may hence be restricted.

IV. MULTI-ROTOR FENCE PERFORMANCE

The multi-rotor fence, consisting of four turbines arrayed in the cross-stream direction as illustrated in Figure 1 with an inter-turbine spacing of $s/d = 1$ ($B_L = 0.1960$) and a global blockage ratio $B_G = 0.0507$, was simulated in a range of operational conditions. The turbines were numbered from 0 to 3 from left to right across the array, so that turbines 0 and 3 are denoted the ‘outboard’ turbines, and turbines 1 and 2 are denoted the ‘inboard’ turbines. The turbines counter-rotate, so that turbines 0 and 2 rotate anti-clockwise, and turbines 1 and 3 rotate clockwise.

The variation in inboard and outboard rotor thrust and power coefficients with tip speed ratio in the multi-rotor fence configuration is shown in Figure 5, with the values that maximise fence power for the different rotor designs summarised in Table III, noting that the tip speed ratio is assumed to be uniform across the fence. As with the single rotor simulations, turbines designed for higher blockage ratio conditions (e.g., Cases 4 and 5) achieve higher levels of thrust and power at lower tip speed ratios than turbines designed for lower blockage ratio conditions, with the lower blockage ratio design turbines (e.g., Case 1) achieving the highest power coefficient of the five different designs as the tip speed ratio approaches $\lambda = 7$. It should be noted however that the maximum power coefficient of the Case 1 turbine fence is less than that achieved by some of the other, higher blockage ratio, turbine designs at lower tip speed ratios.

The maximum thrust and power coefficients of all the turbines, except for the Case 5 turbines (with a design blockage ratio $B_L = 0.1960$), increased from their values in the single turbine simulations in their design blockage ratios. In all cases, turbine performance for the different designs was improved in

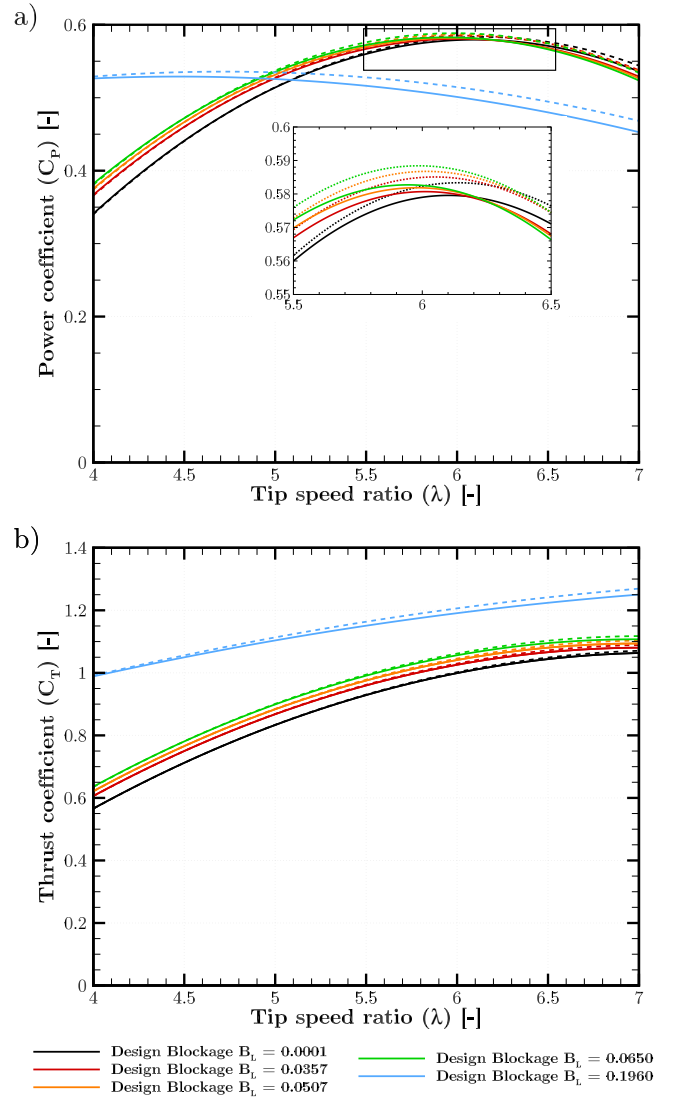


Fig. 5. Variation in (a) rotor power coefficient, C_P , and (b) thrust coefficient, C_T , with tip speed ratio λ for the five rotor designs in the multi-rotor configuration with an inter-turbine spacing $s/d = 1$ ($B_L = 0.1960$), and a global blockage ratio $B_G = 0.0507$. Power and thrust coefficients for inboard rotors are indicated with dashed lines, and solid lines for outboard turbines.

the multi-rotor configuration as compared to single turbine performance in the $B_L = 0.0507$ domain, with the tip speed ratio required for maximum performance slightly lower in the multi-rotor configuration. The increase in maximum power coefficient in the multi-rotor configuration, as compared to the $B_L = 0.0507$ single turbine domain, occurs because, although the global blockage ratio for the multi-rotor fence is the same as in the single turbine simulations, the fence occupies only a small fraction of the overall channel cross-section. The constructive interference that develops between adjacent turbines, increasing the power coefficient, is more significant in the multi-rotor configuration as the turbines are deployed in a more closely spaced configuration, with a local blockage ratio $B_L = 0.1960$. However, in comparison to the

single turbine simulations with $B_L = 0.1960$, the maximum power coefficients of the turbines in the fence configuration are significantly lower (as shown in comparison between Tables II and III), as the maximum resistance that the fence can apply to the flow is limited by the presence of the large bypass flows around the ends of the fence.

In the multi-rotor fence configuration, inboard turbines operate at slightly higher thrust and power coefficients than the outboard turbines, as a consequence of the differing levels of resistance to bypass flow around the inboard and outboard turbines. Closely spacing the turbines in the cross-stream direction within a multi-rotor fence results in the bypass flow around a turbine interacting with the bypass flows around neighbouring turbines, modifying turbine performance. Hydrodynamically, this modification occurs because the increased resistance in the bypass flow means that a higher mass flow rate is sustained through the turbines, for a given level of thrust, and hence power is also increased. The inboard turbines, which are adjacent to other turbines in both cross-stream directions, experience a greater degree of flow confinement than the outboard turbines, which are only adjacent to one other turbine in the cross-stream direction, and the flow can more freely expand in the other, unblocked, direction. The bypass flow resistance is hence lower for the outboard turbines, meaning that the core flow is slightly reduced as compared to the inboard turbines, and hence the thrust and power coefficients of the outboard turbines are slightly lower. The magnitude of the thrust and power coefficient difference between inboard and outboard turbines varies with tip speed ratio, the difference increasing with increasing tip speed ratio, as well as the turbine design blockage ratio. These phenomena occur because when the turbine thrust is reduced, either through operation at a lower tip speed ratio or lower blade solidity (due to a lower blockage ratio design), the acceleration of the bypass is reduced and the effect of the bypass flow resistance on the core flow becomes less significant.

The importance of turbine thrust in the cross-fence variation in power is illustrated in Table III, wherein the lowest design blockage ratio turbines, Case 1 ($B_L = 0.0001$), have the smallest cross-fence variation in power coefficient, with a difference of 0.52% between the inboard and outboard turbines. This difference increases as the design blockage ratio of the turbines increases, with a difference of 0.69% for Cases 2 and 3 turbines, increasing to 0.86% and 1.52% for the higher blockage ratio designs of Cases 4 and 5 respectively. The cross-fence variation in thrust coefficient is relatively constant with design ratio, increasing slightly from 0.3% to 0.4% for Cases 1 to 4, and increasing to 0.74% for the Case 5 turbines. The magnitude of cross-fence power variation is correlated with turbine design blockage ratio because the greater resistance presented by the higher design blockage ratio (and hence higher thrust) turbines means that there is a stronger bypass flow confinement interaction between adjacent turbines. There is hence a greater difference between the bypass flow resistance experienced by the inboard and outboard turbines.

Fence power is the product of two competing effects: the strength of inter-turbine interference effects leading to increased core flow and hence increased turbine power, and the importance of array-scale flow diversion around the multi-rotor fence as the overall fence thrust increases. Consequently, there is a limit to the thrust that can be applied to the fence, be it through the rotational speed of the turbines or turbine design, to maximise overall fence power. The multi-rotor fence with Case 4 turbines ($B_L = 0.0650$) achieved the highest fence power coefficient $C_P = 0.583$ of the five turbine designs. The design blockage in this case is higher than that of the global blockage of the fence, in order to better exploit the inter-turbine interactions due to the close spacing of the turbines within the fence. However, it is lower than the in-fence local blockage ratio which would theoretically best exploit such interactions if the array-scale flow effects were not important, i.e., that the number of turbines in the fence was very large compared to the overall channel cross-section. The optimal turbine design would be expected to change as the number of turbines in the fence increases, as a greater number of turbines would be able to more fully exploit the constructive interference effects between turbines and the reduction in turbine power towards the ends of the fence would become relatively less significant.

A. Fence Performance with Turbine Power Capping

A further consideration in turbine and multi-rotor fence design is performance in operational conditions, such as during rated power operation. Figure 6 shows three contour plots of the streamwise velocity past the multi-rotor fence consisting of turbines of the highest blockage ratio design, Case 5, at three different flow speeds, $u_\infty = 1.80\text{ms}^{-1}$, $u_\infty = 2.00\text{ms}^{-1}$, and $u_\infty = 3.50\text{ms}^{-1}$. Turbine rated power is set to be 500kW, to give a rated fence power of 2MW, so that the rated flow speed is $u_r = 1.81\text{ms}^{-1}$. Below rated flow speed the turbines operate at their hydrodynamically optimal tip speed ratio and power coefficient to maximise turbine power. Above rated flow speed, the blade pitch angle of the turbines is adjusted to pitch the blades towards feather, thereby reducing the angle of attack and thus the axial and tangential forces on the blades, reducing rotor torque and hence maintaining a constant turbine power. It is assumed that rotor tip speed ratio is reduced in order to maintain a constant rotational speed above the rated flow speed.

Figure 6 a) demonstrates that there is significant flow diversion and interaction between the turbines in the fence just below the rated flow speed when the turbines are operated to maximise power takeoff from the flow. At the array-scale, the streamtube encompassing the flow that passes through the fence expands significantly due to the relatively high level of resistance the fence presents to the flow. The flow immediately upstream of the fence is decelerated, and the flow in the array bypass accelerated as it passes the fence location. There is also an extended region of flow remixing behind the turbines. At the turbine scale, the flow speed is substantially reduced immediately behind the turbines, and significant acceleration

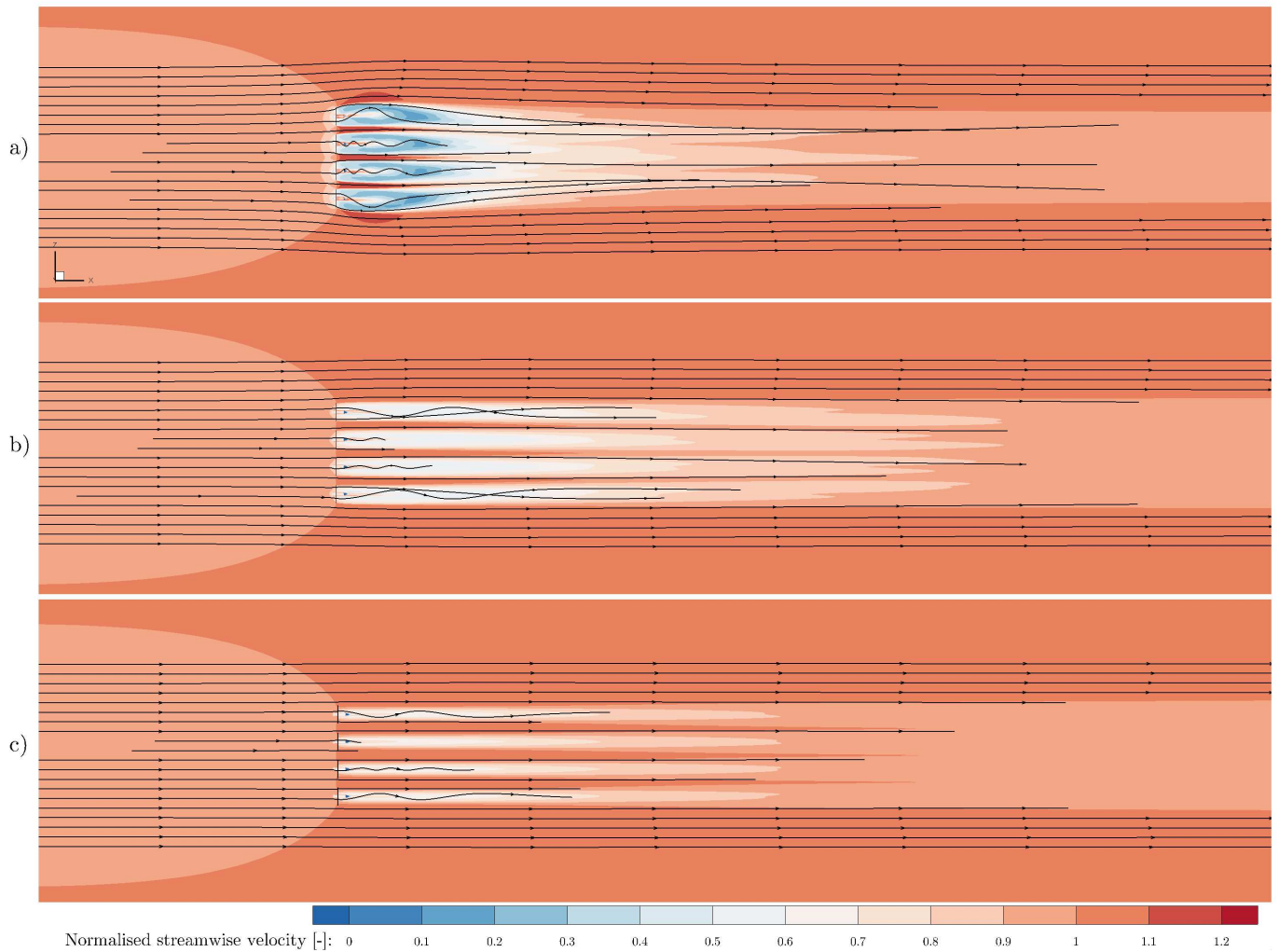


Fig. 6. Contour plot of hub-height streamwise velocity normalised by the reference flow speed past a four turbine fence with turbines of the Case 5 ($B_L = 0.1960$) design for three flow speeds: a) $u_\infty = 1.80\text{ms}^{-1}$, b) $u_\infty = 2.00\text{ms}^{-1}$, and c) $u_\infty = 3.50\text{ms}^{-1}$. Streamtraces have been added help to illustrate fence and turbine flow expansion in each case.

of the flow in the inter-turbine bypass region, with asymmetry between where the bypass flow expands more freely around the outboard turbines than the inboard turbines. This asymmetry leads to the relatively large cross-fence variation in thrust and power coefficients noted previously.

Above the rated flow speed at $u_\infty = 2.00\text{ms}^{-1}$ in Figure 6 b), the impact that the turbines have on the flow, and hence flow diversion around the array is significantly reduced as indicated by the much less significant expansion of the streamtraces passing the fence, because the pitch-to-feather power control acts to reduce both the axial and tangential forces acting on the rotor blades. The reduction in turbine thrust (both in magnitude and coefficient) above rated flow speed means that the difference in bypass flow resistance between the inboard and outboard turbines, while still present, is less significant and hence there is a smaller cross-fence variation in flow speed and hence turbine thrust and power. Increasing the flow speed in the channel further to $u_\infty = 3.50\text{ms}^{-1}$

results in an even greater reduction in turbine thrust, and hence array-scale flow diversion is negligible. At low thrust levels, little flow is diverted around the turbines, and hence the effect of turbines on the resistance to bypass flow acceleration is negligible, meaning that turbine performance characteristics become independent of turbine position within the fence.

The reduction in inter-turbine interference above rated flow speed is a similar effect to that of the low blockage ratio design turbines (e.g., Cases 1 and 2) at low tip speed ratios, where turbine thrust is sufficiently small that interactions between adjacent turbines are relatively small. Consequently, turbine performance in the multi-rotor fence configuration is a function not only of relative turbine placement, but also turbine thrust. The primary advantages of closely spacing turbines within multi-rotor fences therefore comes from harnessing the potential for constructive interference effects to increase the turbine power coefficients and thus achieving rated power at lower flow speeds or a higher rated power at the same flow

speed. Above rated flow speed turbine and fence power is fixed and, with a pitch-to-feather power control system, the interactional effects between turbines reduce. It should be noted that a penalty for closely spacing turbines in the multi-fence configuration is an increase in turbine loads from that which would be expected based on turbine performance in a global blockage ratio matched single turbine domain, or, as turbines are presently evaluated, analysis in an unblocked domain.

V. CONCLUSION

The importance of the blockage ratio in determining the theoretical limit of power of a tidal turbine in a constrained flow passage was demonstrated by Garrett and Cummins [1], showing that the power coefficient increases by a factor of $(1 - B_L)^{-2}$ above the Lanchester-Betz limit if a sufficient level of resistance is applied to the flow. A variety of hydrodynamic limitations mean that tidal turbines cannot exploit the full performance increment implied by the idealised analysis of Garrett and Cummins. However, the physical mechanism by which the blockage ratio leads to a greater streamwise static pressure difference, resulting in improved performance, remains unchanged. For a single device in a blocked flow passage, the implication is that a higher power coefficient than the Lanchester-Betz limit can be achieved if the device is designed and operated to utilise the additional streamwise static pressure gradient that develops in the flow passage in order to increase rotor torque, and thus power.

Single rotor designs for a fixed tip speed ratio $\lambda = 5.00$, hydrodynamically optimised to achieve a constant angle of attack along the blade span to maximise the lift-to-drag ratio, were undertaken in domains for five different blockage ratios, $B_L = 0.0001$ (unblocked), $B_L = 0.0357$, $B_L = 0.0507$, $B_L = 0.0650$, and $B_L = 0.1960$. Blade solidity ratio and blade twist angle were the two degrees of freedom available in the design process, with the solidity ratio increasing as the design blockage ratio increased, accompanied by a very slight reduction in the twist angle along the blade span. Only the highest blockage ratio design exceeded the Lanchester-Betz limit in its design conditions, achieving a maximum power coefficient $C_P = 0.752$, although all turbine designs exceeded the limit when tested in the highest blockage domain, for example, the unblocked design achieved a maximum power coefficient of $C_P = 0.717$. The rotational speed of the turbine at which the peak power coefficient was achieved was higher for the lower blockage ratio turbine designs, as the lower blade solidity of those designs meant that a higher rotational speed was required in order to provide a sufficient level of resistance to the flow to maximise turbine performance. Consequently, constraints on turbine rotational speed, such as those due to cavitation inception concerns and drive train limitations, are likely to have a greater impact on the maximum power achieved by lower blockage turbines, as they generally must operate at higher rotational speeds than higher blockage turbines.

The five turbine designs were evaluated in a four turbine fence, where the turbines were closely spaced with a tip-to-tip spacing of $s/d = 1$ in the cross-stream direction. Turbine performance improved, as compared to the design case, for all turbines (except the most highly blocked design), as the closely spaced arrangement of the turbines within the fence resulted in stronger constructive interference effects between adjacent turbines than would be expected from the design blockage ratios of the turbines. The constructive interference that develops by closely spacing turbines is driven by the interactions of the bypass flows around the turbines. A higher mass flow rate can be sustained through the turbines due to the resistance to acceleration of the turbine bypass flows from the presence of neighbouring bypass flows. Turbines at the ends of the fence, adjacent to only one other turbine, benefit from the increased resistance to bypass flow from only one side, and hence there is cross-fence variation in thrust and power. The magnitude of the cross-fence variation is a function of turbine thrust, with a greater variation being observed at higher tip speed ratio and for higher blockage ratio turbine designs. Similarly, control strategies were shown to affect the cross-fence performance variation with strong interference, and consequently significant cross-fence power and thrust variation, below rated flow speed when the turbines are operated to maximise the power coefficient. Above rated flow speed, the pitch-to-feather control strategy results in a reduction in the axial and tangential blade forces, and hence the interactions between turbines are reduced and they operate more independently of adjacent turbines.

These results have important practical relevance in the design and operation of multi-rotor fences. The primary benefit of designing turbines to utilise the theoretical performance uplift available in a closely-spaced arrangement comes from improving the turbine power coefficient. This results in either increasing the rated power achievable by the design or reducing the rated flow speed at which rated power occurs thus allowing the turbines to operate at rated power over a greater range of flow speeds. Furthermore, designing for flow confinement enables turbines to operate at lower tip speed ratios, which provides a greater safety factor for constraints on rotational speed such as cavitation inception. Above the rated flow speed however the interactions between turbines in a pitch-to-feather power controlled fence reduce.

The optimal blockage ratio for turbine design within a multi-rotor fence is a function of fence length, inter-turbine spacing, and turbine thrust. The constructive interference effects between turbines are stronger for closely spaced, high thrust turbines. The flow may choke and be diverted around the fence if the thrust is too high, as was observed for the $B_L = 0.1960$ design turbines and expected following theoretical models for the power of tidal fences partially spanning wide channels [3]. However, even for a short fence of four turbines, it was found that turbines designed for moderately blocked conditions, $B_L = 0.0650$, greater than the global blockage ratio of the fence, $B_G = 0.0507$, achieved the highest fence power coefficient $C_P = 0.583$ of the five turbine

designs, demonstrating the need to design turbines to support moderately high levels of thrust to maximise the power of the multi-rotor fence configuration.

REFERENCES

- [1] C. Garrett and P. Cummins, "The efficiency of a turbine in a tidal channel," *Journal of Fluid Mechanics*, vol. 588, pp. 243–251, 2007.
- [2] T. Nishino and R. H. J. Willden, "The efficiency of an array of tidal turbines partially blocking a wide channel," *Journal of Fluid Mechanics*, vol. 708, pp. 596–606, 2012.
- [3] C. R. Vogel, R. H. J. Willden, and G. T. Houlsby, "Effect of free surface deformation on the extractable power of a finite width turbine array," *Renewable Energy*, vol. 88, pp. 317–324, 2016.
- [4] S. Draper and T. Nishino, "Centred and staggered arrangements of tidal turbines," *Journal of Fluid Mechanics*, vol. 739, pp. 72–93, 2014.
- [5] T. Nishino and R. H. J. Willden, "Two-scale dynamics of flow past a partial cross-stream array of tidal turbines," *Journal of Fluid Mechanics*, vol. 730, pp. 220–244, 2013.
- [6] J. Schluntz and R. H. J. Willden, "The effect of blockage on tidal turbine rotor design and performance," *Renewable Energy*, vol. 81, pp. 432–441, 2015.
- [7] S. C. Cooke, R. H. J. Willden, B. Byrne, T. Stallard, and A. Olczak, "Experimental investigation of tidal turbine partial array theory using porous discs," in *Eleventh European Wave and Tidal Energy Conference*, Nantes, France, 2015.
- [8] R. Mahu and F. Popescu, "NREL Phase VI rotor modelling and simulation using ANSYS Fluent 12.1," *Mathematical Modelling in Civil Engineering*, vol. 1/2, pp. 185–194, 2011.
- [9] S. C. McIntosh, C. F. Fleming, and R. H. J. Willden, "Embedded RANS-BEM tidal turbine design," in *Proceedings of the Ninth European Wave and Tidal Energy Conference*, Southampton, United Kingdom, 2011.
- [10] H. Glauert, "Aerodynamic theory," in *Airplane propellers*. Julius Springer: Berlin, 1935, pp. 169–360.
- [11] P. Fuglsang and C. Bak, "Development of the Risø Wind Turbine Airfoils," *Wind Energy*, vol. 7, pp. 145–162, 2004.
- [12] A. Wimshurst and R. H. J. Willden, "Computational analysis of blockage designed tidal turbine rotors," in *Second International Conference on Renewable Energies Offshore*, Lisbon, Portugal, 2016.
- [13] A. Wimshurst, C. R. Vogel, and R. H. J. Willden, "Cavitation limits on tidal turbine performance," *Submitted to Renewable Energy*, 2017.